THE RESEARCH INSTITUTE

College of Pure and Applied Sciences

Final Report
NASA Planetology Grant NSG 7420

THICKNESS OF WESTERN MARE BASALTS

Rene A. DeHon
Department of Geosciences

July 1979

(NASA-CR-158784) THICKNESS OF WESTERN MARE BASALTS Final Report (University of Northeast Louisiana, Monroe.) 65 p HC A04/MF A01 CSCL 03B
N79-28101
Unclas
G3/91 29283

NORTHEAST LOUISIANA UNIVERSITY
MONROE, LOUISIANA 71209

NASA PLANETOLOGY GRANT NSG 7420

THICKNESS OF THE WESTERN MARE BASALTS

René A. De Hon

Department of Geosciences
Northeast Louisiana University
Monroe, LA 71209

July 15, 1979

ABSTRACT

An isopach map of the basalt thickness in the western mare basins is constructed from measurements of the exposed external rim height of partially buried craters. The data, although numerically sparse, is sufficiently distributed to yield gross thickness variations. The average basalt thickness in Oceanus Procellarum and adjacent regions is 400 m with local lenses in excess of 1500 m in the circular maria. The total volume of basalt in the western maria is estimated to be in the range of $1.5 \times 10^6 km^3$.

Oceanus Procellarum and the western maria are largely composed of contiguous and superposed circular basins. The youngest basins are readily identified by a large number of basin-related features. Older basins retain progressively fewer identifying features. Mare Imbrium, Mare Humorum, and Mare Vaporum, and Sinus Medii are among those basins which retain a circular outline. Mare Cognitum and Mare Nubium are composite structures of contiguous basins, as is the Flamsteed-Reiner axis of thick basalts in western Oceanus Procellarum. Thick basalt lenses suggest the presence of older, nearly obliterated basins in the Stadius-Sinus Aestuum region as well as in east Oceanus Procellarum adjacent to southwest Mare Imbrium.

The correlations noted between basalt surface features and basalt thickness in the eastern maria prevail in the western maria. Positive gravity anomalies are associated with most thick basalt discs. Mare ridges are located at the sites of buried topographic rises or in zones of transition between thin and thick basalts. Mare domes are located on relatively thin basalts associated with regional rises of the basement topography. Regional variations of basalt surface elevations mimic the subsurface relief. Most rilles are located in thin basalts parallel or subparallel to zones of equal thickness; however, many rilles cut mare material and terra with nearly equal development.

The chief distinction between the eastern and western maria appears to be one of basalt volumes erupted to the surface. Maximum volumes of basalt are deposited west of the central highlands and flood subjacent terrain to a greater extent than on the east. The surface structures of the western maria reflect the probability of a greater degree of isostatic response to a larger surface loading by the greater accumulation of mare basalt.

INTRODUCTION

Mare basalts comprise a significant, but not overwhelming portion of the lunar surface. Basalt covers approximately 20 percent of the surface, but the total volume is less than 1 percent of the total volume of the lunar crust (Head, 1975;). Accurate knowledge of the basalt thickness and distribution yields important constraints to several types of lunar models. Knowledge of the thickness of mare basalts is required to adequately reconstruct pre-flooding surface topography and to establish basalt volumes. The volume of basalt produced during the episode of mare-filling provides important constraints to the lunar thermal history. Establishment of the basalt thickness distribution provides additional parameters in models of lunar gravity and isostasy, paleomagnetic correlations; and impact geochemical mixing. In addition, correlation of regional topographic variations and paletopography supply data relevant to the origin of basalt surface structures.

In previous studies it was shown that the mare basalts in the eastern maria average 200 - 400 m thick with basalt lenses near 1200 - 1500 m in the deeper parts of the basins. This study extends the thickness observations to the western maria. Incontrast to the distinct, isolated mare basins of the eastern maria, the basalts of the western maria merge to form a continuous surface. The large surface area with less confining contacts and significantly less accurate data compound the problem of accurate isopachus construction.

This paper centers on the determination of the thickness of mare basalts and the configuration of the western mare basins. An isopach map is prepared for the region between the limits of 45°N to 45°S and 10°E to 90°W. In addition, a synthesis of regional data, including model paleotopography and the location of basalt surface features is prepared for correlation with the isopach map. This paper is chiefly limited to a discussion of the origins of the data sets, limitations of the data, and presentation of the various map products. Important correlations between data sets are noted.

DATA SOURCE AND METHODS

METHOD

An isopach map has been constructed for the western mare basalts using the crater geometric technique which is on the exposed rim height of craters partially buried by mare basalt (Eggleton, 1963; De Hon, 1974, 1975). The technique is briefly reviewed in order to note the inherent limitations and generalizations of the method.

Fresh impact craters on the moon display diameter-dependent morphological parameters which may be used to reconstruct the original morphology of buried or otherwise deformed craters. Important in the estimation of basalt thickness is the relationship between crater diameter (D) and external rim height (h). The relationship is defined by Pike (1974, 1977) as follows:

(1) $h=0.036\ D^{1.014}$ for craters $<$15 km in diameter

(2) $h=0.399\ D^{0.236}$ for craters $>$15 km in diameter

For partially buried craters, the average diameter and height of the exposed portion of the rim are determined from existing topographic maps or by shadow length measurements. The original rim height is determined from the crater diameter and the appropriate equation (Fig. 1). The original rim height minus the exposed rim height is assumed to be the thickness of material superposed in the vicinity of the crater (Fig. 2).

Pike's equations are derived from averaging variations at single craters. In like manner, two to four exposed rim height measurements were determined for buried craters. Thus the average exposed rim is used in the final thickness estimation.

For most craters, a single thickness estimation is recorded for each crater. For some large craters ($>$ 75 km diameter), more than one thickness value may be determined for widely separated points along the rim. For those craters which occur along the edge of the basin, the thickness estimate is averaged over the flooded portion of the rim and plotted on the rim crest projection into the mare.

Thickness estimates ignore local lensing within the crater interior as well as the wedging-out of mare-material on the outer crater rim rampart. The thickness estimate is thus a generalization of the average basalt thickness within the region of the crater without regard to local variations caused by the buried relief of the crater (Fig. 2). The resulting thickness estimates (Fig. 3) are contoured to produce an isopach map. The isopach map (Fig. 4) portrays regional trends and variations in basalt thickness but does not retain local variations due to the existence of individual buried craters.

The isopach map (Fig. 4) is constructed from 142 interior thickness estimates and 148 points to define the limits of the mare-material and major intrabasinal, nonflooded terrains. The data distribution is an uneven scatter of points ranging from 1 point per 1^{o} radius to 1 point per 20^{o} radius. Thus the precision of contouring is variable over different regions of the map.

A preliminary isopach map was produced with a contouring program using a 5^{o} search radius around each point to construct a 1^{o} grid of the data. A seven point, 2^{nd} order polynomial smoothing function was used to contour the gridded data. Some areas of the map could not be adequately constructed by this program; hence, hand-contouring was required to adjust isopach lines to some sparse regional data. The final isopach map was hand-contoured on the 1:5,000,000 mercator base map. An attempt was made to honor all data points; however, a few points could not be included in the final draft and some isolated data points may impose significant but dubious features on the map. Trend surface analysis up to the 8^{th} degree failed to provide a significant match of the data. Harmonic surface analysis may provide an acceptable display of the larger trends and features of the region, but was not attempted for this study.

LIMITATIONS AND ACCURACY

The accuracy of the isopach map is dependent on several factors, not all of which can be fully known or controlled. The following are optimum conditions:

1. Data spacing and density are sufficient to construct isopach lines;

2. Relief data at crater rims are accurate;

3. Buried craters maintain the morphology of fresh craters;

4. Buried craters selected for thickness measurements are superposed on the basin floor beneath mare material.

Partially buried craters which comprise the data population are necessarily scattered with a random distribution and variable density of data points. Inasmuch as craters occupy large areas (10-100 km in diameter), the thickness estimate at any one crater represents an average thickness over a substantially larger area. Further, the number of partially buried craters preserved in a region is a function of the original crater density in the area, crater size, and thickness of superposed materials. Large numbers of small craters of low relief are lost by total submergence (burial) while only the larger craters are preserved. Hence, as the thickness of the superposed materials increases, the point density of data decreases. As the thickness of superposed materials approaches 1.5 km most craters are obliterated. Hence, thick lenses of material within deeper basins cannot be measured by a crater geometric technique.

The accuracy or reliability of any map is dependent in part on the spatial distribution of the data points. A point distribution coefficient based on the nearest neighbor method is used to determine how representative the distribution is of a population (Morrison, 1970). The coefficient is calculated by the equation:

$$R = \bar{D}(o)/D(e); \quad \bar{D}(o) = \frac{\Sigma d(i)}{N} \quad \text{and} \quad \bar{D}(e) = \frac{\sqrt{A/N}}{2}$$

where: $\bar{D}(o)$ is the mean point distance of the observed distribution

$\bar{D}(e)$ is the mean point distances of a random distribution

$d(i)$ is the distance from any point to its nearest neighbor

A is the area

N is the number of points.

The point distribution coefficient ranges from 0.0, when all points are clustered at the same location, to 2. 15, when the points have their mazimum spacing in a regular hexagonal pattern. The coefficients can be classed into the following types of distributions:

COEFFICIENT	TYPE
0.00 - 0.90	Clustered to random
0.91 - 1.25	Random
1.26 - 2.15	Random to uniform

Greatest confidence is placed in data with coefficients above 1.25, and little confidence is placed in coeffients below 0.90.

The overall point distribution coeffient of the western maria is 1.2 with extremes ranging from 0.87 to 1.39 (Table I). The distribution is random and within the range of useful data. A qualitative check on the overall reliability of the data distribution is provided by the apparent sensibility of the data in correlation with other types of information.

The relief data at crater rim crests are derived from three sources. Where Apollo mapping camera stereographic frames exist, topographic maps provide coverage with contour intervals of 50 or 100 m. Spot elevations at some craters provide elevation differences in meters. The error of elevations from orbital photogrammetry is approximately 30 m. In regions beyond the zone of Apollo mapping frames

(Fig. 3) relief information is obtained from earth-based photogrammetry as incorporated in the Lunar Aeronautical Charts or shadow length calculations from Orbiter Frames. These data incorporate an average error of approximately 100 m. The accuracy of the relief data is thus variable and less than comparable studies of the eastern maria (De Hon and Waskom, 1976) which derived the bulk of the data base from Apollo Lunar Topographic Orthophotographs.

A fundamental supposition in estimating the thickness of basalts requires that the flooded crater maintain the essential morphologic and geometric parameters of an average fresh crater. Three basic assumptions exist in regard to crater morphology: 1) the crater is reasonably undegraded at the time of flooding; 2) the crater follows the morphologic trends of craters used to obtain the descriptive function of rim height and diameter; and 3) emplacement of mare basalt does not significantly alter the original crater geometry. These assumptions are the major unevaluated factors involved in the thickness determinations. The remainder of this section is devoted to points which tend to support an a priori argument that buried craters retain a fresh crater morphology.

The residence time of an unburied crater is limited to a restricted time interval. All craters used in the estimates formed prior to the beginning of Eratosthenian time. Most are Imbrian in age (e.g. formed on early Imbrian surfaces and covered by late Imbrian basalts). Some craters are Nectarian in age, hence, existed for somewhat longer resident times before burial. Burial by basalt emplacement inhibits further degradation. It is assumed that these craters are, for the most part, preserved with little to moderate degradational effects. Many Imbrian craters of the highlands maintain crater morphologies close to those of Eratosthenian or Copernican craters.

Hörz (1978) argues that a closer approximation of preserved crater geometry is obtained by using degraded crater morphologies. He estimates that these values are approximately one-half of the fresh crater values. Thus, the resulting isopach map (Hörz, 1978) shows one-half the thickness obtained for the western maria (De Hon, 1978) and for the eastern maria (De Hon and Waskom, 1976). I agree, in general terms, with the principle that the use of fresh crater equations may tend to overestimate the basalt thickness. I oppose a nonspecific overall reduction of all thickness values because many craters must retain fresh crater morphology. It does follow that true thickness may be less than that recorded for some areas. If an error is introduced, I would prefer the error be retained on the thick side and not an unevaluated spread of error which allows thickness to be either thicker or thinner at any one point.

Pike's (1977) equations for crater geometries involve averaging rim heights at several points for any one crater. A regression line is fitted to the average value of a large number of craters. Crater thickness estimates use average rim height as well as multiple thickness estimates where possible to minimize error introduced by variability in the data. However, not all fresh craters follow the established trends. Notable exceptions in diameter vs rim height trends do occur (for example Taruntius, Ritter, and Sabine). No precaution can exclude craters which do not follow the ideal trend. Presumably, the number of these craters is relatively small, and the effect of inclusion in the data set is minor and offset by nearby estimates. The use of these craters gives values which are too thick, because as a group all exhibit rim heights that are less than normal fresh craters.

The emplacement of mare material may alter original crater morphology. The mechanism by which mare material invades crater interiors is not fully known. For some flooded craters with incompletely exposed rim crest, flooding could be a simple matter of overflowing of the lowest elevation of the rim. For those craters with flooded interiors but without breached rims (e.g. Archimedes), the basalts must be emplaced by effusion of basalt from beneath the crater floor. It is reasonable to expect floor modification (Schultz, 1976a and 1976b) and accompanying changes in crater internal geometry. The extent to which the exterior rim geometry is altered, if at all, is not known. For most "floor-fractured craters" which are assumed to have been altered by subsurface magmas (Schultz, 1976b), the rim crest is lower than that of normal craters; therefore, as a general rule, a thickness estimate incorporating these craters may be too thick. However, many craters (e.g. Archimedes) provide evidence that the rim geometry is essentially unchanged by flooding.

The final factor affecting the accuracy of the data is the supposition that the selected buried craters are sitting on the pre-mare basement and not formed on intrabasalt surfaces. Earth-based and lunar orbital spectral studies offer a potential means of verification of the stratigraphic horizon of crater formation. The rim ejecta of those craters formed on the pre-basalt surface may be identified as composed of highland-type material (McCord *et al.*, 1972). Both the limiting resolution of the spectral techniques and the small numbers of buried craters studied limit the contribution of this data to the study at this time. Nevertheless a few identified pre-mare craters in Oceanus Procellarum provide tie points for the larger framework of unverified data.

Further limitation on the estimates of thickness of basalt is imposed by those post-mare (Eratosthenian and Copernican) craters which have been excavated through the basalt to eject pre-mare terra materials. These craters may be identified by the highland component of their ejecta (McCord *et al.*, 1972; Andre *et al.*, 1979). Resolution and dilution effects severely limit the number of craters presently identified. As an example, the crater Kepler was originally classified as a post-mare crater that did not exhibit evidence of excavation beneath the basalts; hence, the basalts would have had to be thicker than the true depth of excavation (approx. 2km, McCord *et al.*, 1972). Recently obtained data establishes the presence of highland material in the rim ejecta (Pieters, 1977); hence, the basalt thickness is less than 2km. Post-mare crater spectra will be of major importance when the resolution allows identification of highland components in the smallest craters to penetrate the basalts. Orbital x-ray flourescent spectra have established the presence of highland components in several post-mare craters in the eastern maria (Andre et al., 1979). Gamma ray spectra have been used to identify non-mare ejecta from Lambert and Timocharis in South Imbrium (Metzger et al., 1979).

It is hoped that improved resolution spectral reflectance studies of pre- and post-mare craters will allow selection and final verification of most craters used in the construction of the isopach map. A qualitative argument for the essential accuracy is demonstrated by consistent trends of data and correlations of the isopach data with other types of physiographic data. In some mare regions, buried craters of various sizes are identified within a single locality. Often these craters give inconsistent thickness estimates. Small buried craters are most likely resting on intra-basalt surfaces while the larger craters are resting on the basin floor. Hence, large craters generally give more consistent results.

MAP PRODUCTS

WESTERN MARE PROVINCES

The western maria are subdivided into seven regions (Fig. 5), each of which is characterized by one type of dominant subsurface structure or related structures. The surface morphology of each of these regions is sufficiently distinct to allow description of each subdivision in terms of surface characteristics. The provinces are similiar to those of Hackman and Mason (1961). The mare provinces are used as convenient regional subdivisions for describing the results of this study. The seven provinces are defined as follows:

Imbrium Basin-The Imbrium basin is defined by a ring of mountains which rise as much as 5000 m above the mare surface. The basin ring is composed of Montes Carptus, Montes Apenninus, Monte Caucasus, Montes Alpes, and Montes Jura. The ring is breeched in three places; in the south between the Carpatus and Apenninus sections, in the east opening to Mare Serenitatus between the Apenninus and Caucasus sections, and on the west (almost a quarter of the basin circumference) between the Jura and Carpatus sections. Sinus Iridum forms an embayment on the northwestern rim. The 1300 km diameter Imbrium basin is the largest circular basin on the lunar surface and one of the youngest multi-ringed basins.

Northern Procellarum - The rather featureless mare plain of Northern Procellarum contains the large crater remnants of Struve, Eddington, and Russel to the southwest. The Rumker Hills are the most prominent features near the center of the region.

Eastern Procellarum- This region is west of the Imbrium basin adjacent to the largest segment of breeched Imbrium rim. The mare plain contains the Aristarchus Plateau and Montes Harbinger to the north and extends south to the Milichus Domes.

Western Procellarum- The Western Procellarum province extends along the western reaches of Oceanus Procellarum from south of Struve to north of Mare Humorum. This region includes the Marius Domes, the buried crater Flamsteed P, and a prominent linear trend of mare ridges.

Central Lowlands- This region consists of the mare lowlands south of Mare Imbrium. Several diverse and independent basins are included in this composite of lowlands. The lowlands include Sinus Aestuum, Sinus Insularum Mare Vaporum, Sinus Medii, and Mare Cognitum.

Nubium Basins- Mare Nubium is a composite basin east of Mare Humorum and south of Mare Cognitum. The region includes Palus Epidemiarum to the south and is limited by the Central Highlands to the east.

Mare Humorum- This small province consists of the circular disc of mare plains in the Humorum basin. The basalt plains are surrounded by an ill-defined ring of mountains or rugged terrain which is breeched on the east and northeast.

ISOPACH MAP

The thickness of basalts in the western maria are depicted with an isopach interval of 250 m (Fig. 4). The resolution over two-thirds of the map is sufficient to portray significant thickness variations over a 5^{o}area and most lensing occurs over a range of $5^{o}$to 10^{o} or larger. The average thickness of basalts in the western maria is approximately 400m which represents an approximate volume of material on the order of 1.5×10^{6} km^{3}.

The major features of the isopach map are thickening discoidal and prismatoidal deposits of basalts and notable regions of basalt thinning. The major areas of discoidal lenses correspond to identified large circular basins such as Humorum, Cognitum, and Imbrium. The maximum thickness of basalt in the younger circular basin is not known because of the lack of preserved buried craters, which generally indicates a thickness in excess of 1500m. Other lenses correspond to regions which have been suggested as basins based on incomplete surface features. At least one new buried basin is revealed by the thickening disc in the Eastern Procellarum Province (23^{o}N; 59^{o}W).

Attempts to produce an isopach map of the Imbrium basin basalt have been frustrated by the limited number of data points and computer contouring resulting in a portrayal of an irregular lens thickening only slightly toward the center and many local irregularities. The final model of the basalts in the Imbrium basin (Fig. 4) is constructed using auxillary data input as a constraint to the isopach form. A two ringed, nested crater is portrayed based on the location of mare ridges and isolated massifs (De Hon, 1979).

Northern Procellarum is lacking in sufficient data for a well defined picture of its probable basalt distribution. The spotty data suggest that the region as a whole is covered by relatively thin basalts with local irregularities. The existence of a 700 km diameter basin at 27°N;72°W in the region of Struve (Howard et al.,1974; Scott et al.,1977) is not apparent in the thickness map (Figs. 4 and 5). If a basin did exist in this region it is degraded beyond present recognition.

The amount of information for the remainder of the map (Fig. 4) allows the isopach map to be constructed with a higher degree of confidence. The East Procellarum Province contains a relatively thick lens of material adjacent to the large gap in the southwest rim of Imbrium. The Western Procellarum Province has the form of a long irregular prism of basalt reaching 1000-1500 m thick in at least three centers of accumulation. The composite nature of the Central Lowlands is evident by thick lenses in Mare Cognitum and Sinus Aestuum contrasted with thinning of basalts southwest of Montes Carpatus and in the Fra Mauro region. Mare Humorum is a simple discoid lense, but the Nubium Province is more complex (De Hon, 1977)

SURFACE TOPOGRAPHY

Topographic information for the western portion of the earth-facing hemisphere is highly variable. The Apollo Metric Camera photography and laser altimetry is limited to narrow strips crossing southern Imbrium-Northern Procellarum and Mare Cognitum-Southern Oceanus Procellarum. All other information has been acquired by Orbiter spacecraft or photogrammetry of earth-based telescopic photographs. The LAC topographic maps provide useful relief data, but are of questionable value for regional information. As a first approximation of possible regional correlation of surface topography and mare thickness, comparison is made with the 12th degree harmonic topographic model (Bills and Ferrari, 1977).

The model topography is portrayed with a 500 m contour interval and a resolution of approximately 10 degrees (Bills and Ferrari, 1977). The resulting map (Fig. 6) resolves most of the major regional scale topographic variations within the area of investigation, but averaging of high frequency data within large sampling areas does lose 2-4 km from the maximum and minimum elevation of the surface in the region of Mare Imbrium. The topographic model does deplict the troughing along the axis of western Oceanus Procellarum and a broad swell in the Central Lowland Province. Unfortunately, Mare Humorum and the Nubium region are not readily distinguishable from the surrounding regions. The terra regions, however, are shown as areas of higher terrain.

Previous attempts to portray regional or global lunar surface topography vary considerably in detail and absolute elevations (for example: Baldwin, 1963; Army Map Service, 1960; ACIC LAC Topographic Maps) but similar trends are common to most maps. The circular basins exhibit depressed centers; the Western Mare Province is a linear topographic depression; and the central highlands are an elevated region. It is significant that where more detailed topography is available, thick lenses of basalt are almost invariably marked by a topographic low.

SUBSURFACE TOPOGRAPHY

As a first approximation of the pre-basalt paleotopography the isopach map (Fig. 4) is subtracted from the 12th degree harmonic topographic map (Fig. 6). The results, contoured with a 500m contour interval, portray a model of the surface topography with the basalt removed (Fig. 7). _If_ the topographic model is accurate and _if_ isostatic compensation has not taken place in response to the basalt, then the map portrays the lunar surface prior to the emplacement of the basalt. Unfortunately, any short-comings of the topographic model are included in the subsurface model.

Nevertheless, the "shoreline" is reasonably represented by the -1500m contour line. Most of the identified basins are included on the paleotopographic model. Inasmuch as there is an approximate overall correlation of basalt thickness and surface elevation, the effect of the subtraction is to accentuate depressions.

The paleotopographic model (Fig. 7) is characterized by depressed surface with maximum relief in excess of 5500 m from mid-Imbrium basin to the Central Highland bulge. Individual basins are portrayed as roughly subcircular depressions 1000 m to 2500 m deep. Actual depths are probably somewhat greater since the harmonic model tends to lose maximum and minimum elevations (Bills and Ferrari, 1977).

On a regional scale, most of the Procellarum basin forms a large arcuate trough which runs from the northwestern edge of the map south and southeast in to the Nubium basin. The trough is a significant constituent of the pre-flooded terrain, but its genesis is largely problematical. The trough may represent a chance alinement of basin-sized impacts, or some sort of a mega-circum-Imbrium trough.

The Imbrium basin dominates the northeastern portion of the map. The basin is revealed as a discontinous ring of raised topography (above -2000m elevation) surrounding a broad shelf (-2500 to -3000m level). A relatively deep inner basin (elevations less than -3000 m) occupies the basin center. The scale, contour interval, and generalized nature of the map does not allow adequate representation of the prominent inner ring of the basin between the shelf and inner basin.

SYNTHESIS

SURFACE FEATURES.

A sketch map of the major mare surface features is presented for comparison with the isopach map and related map products. This map (Fig. 8) shows the location of the major rilles, mare ridges, and domes. The data base for the surface maps is a composite and simplification of the surface features depicted on the 1:1,000,000 geologic maps of the moon and the 1:2,500,000 synthesis map of Scott *et al.* (1975). A close correlation between the location of mare surface structures and thickness trends was demonstrated for the eastern maria (De Hon and Waskom, 1976). The more extensive basalt flooding and the scarcity of interbasinal highland materials make this an even more significant study in the western maria. Many of the major surface trends do show significant correlations with the isopach map and/or subsurface model. Some features, which do not show the expected correlations, may point to unsatisfactory models of basalt thickness or to incompletely understood control mechanisms.

Arcuate rilles invariably are located in regions of thin basalts. They are usually close to the edge of the basin and parallel or subparallel to it. Most are confined to the basalts, but unlike the rilles of the eastern maria many rilles transect both mare material and highland material. Notable examples of this class are the rilles of the Rimae Hippalus set which are outside of and concentric to the southeast raised rim of Mare Humorum. The rilles belonging to the Rimae Bradley and Fresnel sets in Mare Imbrium are parallel to the Montes Apenninus Scarp, but they transect pre-mare material.

There is a concensus of opinion that mare rilles are graben developed in response to tension at the edges of the basins (Baldwin, 1963; Quaide, 1965; Smith, 1966; McGill, 1971). The preferential location in thin basalts (Fig. 8) is consistent with an origin requiring shallow stresses decoupled from the underlying basement (De Hon and Waskom, 1976). Specifically, the intersection of faults bounding a graben marks the contact between crustal materials of contrasting properties (McGill, 1978). Recent studies of the probable depth to the discontinuity based on fault intersections yields estimates ranging from 1.5 to 3 km (Golombek, 1978). There appears to be no significant difference between mare or terra rilles. Hence, the decoulement is probably at the base of the lunar megabreccia (Golombek, 1978) and not at the contact between mare basalt and megabreccia. The tensional stress field may be imposed by basalt consolidation and volume reduction (Swanson and Peterson, 1972; De Hon and Waskom, 1976) or subsidence of the basin in response to the load imposed by the basalt (Melosh, 1978).

Sinuous rilles generally occur over thin basalts near the periphery of thickening wedges, often associated with regions of domes. Most sinuous rilles follow the slope of the surface. Hence they appear to originate in regions of thin basalts and run into topographic lows over thicker basalts.

Domes are largely concentrated in a few broad regions also characterized by thin basalts over subsurface highs. The largest concentration of domes occurs in the Marius Hills region of western Procellarum on the edge of a thick lens of basalt. The Milichus domes occur southeast of Mare Imbrium on the crest of a broad subsurface ridge which divides the East Procellarum and Central Lowland Provinces. The Aristarchus Plateau is located at the edge of the shallow North Procellarum shelf adjacent to the East Procellarum basin. Domes of Mons Rumker are located in apparently thin basalts of the Northern Procellarum Province.

Sinuous rilles and domes are in part closely correlated in time and space with each other and both are correlated to regions of thin mare basalts or topographic highs of the basement floor. Sinus rilles appear to be associated with the latest source vents for young mare basalts (Shaber, 1973). Whether domes and sinuous rilles are products of escaped lava from shallow local residual magma pockets (De Hon and Waskom 1976) or an indication of deeper crustal conduits to the surface is unresolved at this time. Whitford-Stark and Head (1977) suggest that the Marius and Aristarchus volcanic complexes may be the source vents for much of the central Procellarum mare fill.

Mare ridges exhibit preferential locations similar to the controls observed in the eastern maria (De Hon and Waskom, 1976). Concentric trends within the well-defined circular basins of Humorum and Imbrium are apparent. Other partial arcs and circular patterns are observed associated with thick lenses of basalts which mark the location of totally flooded basins such as the west Nubium basin and those of western Procellarum. The western Procellarum Province is characterized by a broad trough with a linear trend of mare ridges on either side of the trough axis. For the most part, mare ridges are located along zones of changing basalt thickness (e.g. areas of maximum paleoslope) adjacent to the thickest lenses.

There is less concensus as to the origin of mare ridges. Hypothesis of mare ridge origin include: (1) draped subjacent topography (Baldwin, 1963; Maxwell et al. 1975); (2) intrusive or extrusive volcanism including auto intrusion (Whitaker, 1966; Strom, 1972; Hodges, 1973; Scott *et al.*, 1975); (3) tectonic deformation resulting from isostatic subsidence or mascon loading (Bryan, 1973; Melosh, 1978); and (4) tectonic formation due to crustal compression accompanied by thrusting (Shaber, 1973; Howard and Muehlberger, 1973). A combination of processes is favored by Tjia (1970), Hartman and Wood (1971), Colton *et al.* (1972) and De Hon and Waskom (1976). Many of the suggested origins are not mutually exclusive. The preferential location of mare ridges in zones of changing basalt thickness

(Fig. 4 and 8) provides at least partial control for subsiquent hypotheses of origin. Mare ridges are largely surface features (probably compressional) localized by the configuration of the basin floor (Fig. 7).

CIRCULAR BASINS AND RELATED STRUCTURES

Oceanus Procellarum and the western maria are largely composed of superposed or contiguous circular basins (Fig. 9). The youngest basins are readily identifiable by a large number of basin related features such as complete to partial arcuate raised rims, relatively thick basalt lens, concentric ridge patterns, and positive gravity anamolies. Older basins retain progressively less features and identification eventually becomes problematical.

Most of the larger basins probably have inner rings and a nested-crater structure. Humorum, Nubium, and the northern-most West Procellarum basin exhibit partial arcs of mare ridges which occupy the inner ring location. However, the scale of isopach construction and data spacing does not allow reconstruction of the complex inner structure (Fig. 4). Most basins are portrayed as simple, thickening discs. Table II lists 14 probable basins of the region. Mare Imbrium occupies the largest and youngest of the basins. Mare Humorum, Mare Vaporum and Sinus Medii are among those which still retain an identifiable circular outline. Mare Cognitum is probably a composite of two small basins with small segments of the rim preserved as Montes Riphaeus and isolated terra patches around the periphery. Mare Nubium is a composite structure comprised of adjacent basins (De Hon, 1977).

Other regions are chosen as probable basins on the basis of incomplete arcs of terra contact, mare ridge patterns, or thickening lenses of basalt. The isopach map (Fig. 4) confirms or lends support to the presence of basins in Sinus Aestuum, the Flamsteed region (6°S;43°W), and northern West Procellarum (8°N;59°W). The existance of a basin in the region of Struve (26°N;72°W) is not confirmed by a measurably thick lens of basalt; however, the scalloped nature of the mare-terra contact and an arcuate mare ridge pattern are suggestive of a basin.

The identification of a relatively thick lens of basalt in the East Procellarum region (23°N;36°W) points to a probable pre-Imbrian basin in this region. The existence of the East Procellarum basin helps explain the otherwise enigmatic break in the southwest rim of the Imbrium basin.

Circum-basinal troughs (De Hon and Waskom, 1976) are not abundant, but at least partial arcs of lowlands may be observed around some of the basins (Fig. 4 and 9). Palus Epidemiarum is flooded terrain at the intersection of a circum-Humorum and circum-Nubium trough (De Hon, 1977). Short fragments of troughs may be recognized around the West Procellarum basins. Northern Procellarum connects with Mare Figoris which forms a well-defined arc of lowland circumferential to Mare Imbrium.

LUNAR GRAVITY AND BASALT THICKNESS

No attempt is made in this study to quanitatively correlate gravity and basalt thickness. However, some qualitative comparisons are significant. Major mascons (Muller and Sjogren, 1968) are associated with the youngest, large circular basins. Mare Imbrium exhibits a 180 mgal positive anamoly, and Mare Humorum exhibits a 160 mgal anamoly. A small, +20 mgal linear trend in western Procellarum is coincident with the trough of thick basalts. Sinus Medii and the Sinus Aestruum-Stadius region are both characterized by +20 mgal anamolies.

From a first assumption of a single dense buried mass (Stripe, 1968; Urey, 1968) to a more complex model of relief at the lunar mantle (Wise and Yeats, 1970; Philips et al., 1972) a comprehensive model of lunar interior structure and gravity is gradually emerging. The mare basalts are largely superisostatic loads imposed on an otherwise isostatically compensated surface (Bowin et al., 1975). The observed gravity variations are the combined results of relief of the lunar mantle formed in response to early topographic irregularities (such as basins) plus the added effects of an uncompensated load imposed by basalts emplaced on a rigid surface.

Thurber and Solomon (1978) have produced several models of crustal structure to match lunar gravity. One model (Fig. 10) involves superisostatic basalts. While this model does not conform in detail to the basalt thicknesses derived in this study, it does agree in magnitude and overall characteristics. Apparent discrepancies between the photomorphometric and gravity-derived thickness may point to regions of partial isostatic compensation after basalt emplacement.

The extent to which isostasy has modified the surface of the basalts remains an unsettled point. The pre-basalt basins were almost certainly brought into isostatic equilibrium (Thurber and Solomon, 1978). Whether post mare-fill isostatic adjustments have occurred, and to what extent, is a significant factor in attempting to reach agreement between photogeologic and geophysical models. Some isostactic subsidence of the basalts is required by various models of mare ridges and rilles (Howard and Muehlberger, 1973; Thurber and Solomon, 1978).

Isostatic subsidence appears to be the most logical mechanism to form the concentric rille pattern southwest of Mare Humorum (De Hon, 1977). Not all surface subsidence need be isostatic, rather some subsidence may be the result of volume reduction of lavas by outgasing and consolidation (Cruikshank *et al.*, 1973; De Hon and Waskom, 1976).

SUMMARY AND DISCUSSION

The basalts of the western maria occupy large circular basins and surrounding lowlands associated with the basins. While Mare Imbrium and Mare Humorum are the only well-preserved circular basins, isopach mapping reveals that even the vast expanse of basalt plains of Oceanus Procellarum mantles a composite structure of several coalescing basins. The thickest basalts are found in Mare Imbrium, Mare Humorum, and the western part of Oceanus Procellarum. Relatively thin basalts are found south and southwest of Mare Imbrium in the Central Lowland region and in Northern Procellarum. The average thickness and total volume of basalts in the western basins is greater than that of the eastern maria.

For the most part, the general conclusions of the earlier studies of the eastern maria are confirmed in the western maria. These conclusions are as follows:

1. The basalts are relatively thin, averaging approximately 400m thick, with thickening discs associated with major basins.

2. Younger basins contain thicker accumulations of basalt than older basins.

3. Isopach mapping confirms the existence of previously proposed buried basins and has identified regions of probable unidentified basins.

4. Rilles tend to be located in relatively shallow mare basalts parallel or subparallel to zones of equal thickness.

5. Mare ridges tend to be located at the site of buried topography or in regions of maximum variation in basalt thickness (e.g. transition between thin basalts and thick lenses).

6. Domes tend to be located on relatively thin basalts associated with regional rises of the basement topography.

7. Regional variations of basalt surface elevations mimic (at a lesser relief) subsurface topography.

8. Positive gravity anomalies tend to be associated with the thickest basalt lenses in circular basins, but not all probable basins exhibit gravity anomalies.

A few notable and possibly significant exceptions to these generalizations are found in the western maria. The exceptions may provide as much insight into the structural regime and history of the maria as the general trends. These exceptions are as follows:

1. Many arcuate rilles are not restricted to mare basalts, but cut highland and mare material with equal development. These rilles must be related to regional tensional stresses affecting basement materials.

2. The mare ridge pattern in Northern Procellarum is not associated with an identified thickening lens.

Any comparison of the eastern and western maria draws attention to a distinct character in the distribution of mare materials. The eastern maria comprise less surface area and the composite nature is apparent. The eastern basalts are more discontinuous being restricted to basins and lowlands with only minor overflow connecting the basalt surface. On the other hand, the western maria are connected by an almost continuous surface of basalts over a much larger area. The prime distinction between the eastern and western maria appears to be one of basalt volumes. The western basins and adjacent terrains are submerged by a thicker mantle of basalts.

The mare basalts are emplaced in low lying terrain which forms an inverted yoke around the Central Highland earth-directed bulge. Maximum volumes of basalt are deposited west of the Central Highlands flooding the terrain to a greater extent. Surface structures such as rilles and ridges are restricted to the mare basalt in the eastern maria and can be interpreted as primarily formed by stresses internal to the basalts. Similar structures of the western maria transect mare-basalts and highland material; hence they must be related to less restrictive stresses. The western maria and related surface structure may reflect the probability of a greater degree of isostatic response to a larger surface loading by the thicker basalts.

ACKNOWLEDGEMENTS

This work was supported by NASA Grant NSG 7216 at the University of Arkansas at Monticello and NASA Grant NSG 7420 at Northeast Louisiana University. The help of Mrs. Nell Cooley and Mrs. Janice K. Ledoux is gratefully acknowledged. Mr. John B. Sharp, Miss M. Denise Young, and Miss Susan Glenn also provided valuable assistance.

References

Army Map Service (1960) Topographic lunar map, Edition 1-AMS, 6 sheets.

Andre C. G., Wolfe R. W., Adler I., and Clark P. E. (1979) Mare basalt depths from Orbital x-ray data. In lunar and planetary Sci X p. 38-40. The lunar and Planetary Institute, Houston.

Baldwin R. B. (1963) The measure of the moon. University of Chicago Press. 488pp.

Bills B. G. and Ferrari A. J. (1977) A lunar density model consistent with topographic, gravitational, librational, and seismic data. J. Geophys. Res. 82, 1306-1314.

Bowin C., Simon B., and Wollenhaupt W. R. (1975) Mascons: a two-body solution. J. Geophys. Res. 80, 4947-4955.

Bryan W. B. (1973) Wrinkle-ridges as deformed surface crust on ponded mare lava. Proc. Lunar Sci. Conf. 4th, p. 93-106.

Colton G. W., Howard K. A., and Moore H. J. (1972) Mare ridges and arches in southern Oceanus Procellarum. In Apollo 16 Prelim. Sci. Rep., NASA publication SP-315, p. 29-90 to 29-93.

Cruikshank D. P., Hartmann W. K., and Wood C. A. (1973) Moon: "Ghost" craters formed during mare filling. The Moon 7, 440-452.

De Hon R. A. (1974) Thickness of mare material in the Tranquillitatis and Nectaris basins. Proc. Lunar Sci. Conf. 5th, p. 53-59.

De Hon R. A. and Waskom J. D. (1976) Geologic structure of the eastern mare basins. Proc. Lunar Sci. Conf. 7th, p. 2729-2746.

De Hon R. A. (1977) Mare Humorum and Mare Nubium: Basalt thickness and basin-froming history, Lunar Sci. Conf. 8th, p. 633-641.

De Hon R. A. (1978) Maximum thickness of materials in the western mare basins. In Lunar Science IX, p. 229-231. The Lunar and Planetary Institute, Houston.

DeHon R. A. (1979) Structural model of the Imbrium basin. In Lunar Science X, p. 271-273. The Lunar and Planetary Institute, Houston.

Eggleton R. E. (1963) Thickness of the Appenninian Series in the Lansberg Region of the moon. Astrogeologic Studies annual progress report, Aug. 24, 1961, to Aug. 24, 1962. U. S. Geological Survey open file report, p. 19-31.

Golombek M. P. (1979) Structural analysis of lunar grabens and the shallow crustal structure of the moon. J. Geophys. Res. (in Press).

Hackman R. J. and Mason A. C. (1961) Engineer special study of the surface of the moon. U.S. Geol. Survey Misc. Geol. Inv. Map I-351.

Hartmann W. K. and Wood C. A. (1971) Moon: Origin and evolution of multiring basins. The Moon 3, 3-78.

Head J. W. (1975) Lunar volcanism in space and time. Rev. Geophys. Space Phys. 14, 265-300.

Hodges C. A. (1973) Mare ridges and lava lakes. In Apollo 17 Prelim. Sci. Rep., NASA publication SP-330, p. 31-12 to 31-21.

Hörz Friedrich (1978) How thick are lunar mare basalts? Lunar Planet. Sci. Conf. 9th, p.3311-3332.

Howard K. A. and Muehlberger W. R. (1973) Lunar thrust faults in the Taurus-Littrow region. In Apollo 17 Prelim. Sci. Rep., NASA publication SP-330, p. 31-22 to 31-25.

Howard K. A., Wilhelms D. E. and Scott D. H. (1974) Lunar basin formation and highland stratigraphy. Rev. Geophys. Space Phys. 12, 309-327.

Maxwell T. A., El-Baz F., and Ward S. H. (1975) Distribution, morphology and origin of ridges and arches in Mare Serenitatis. Bull. Geol. Soc. Am. 86, 1273-1278.

McCord T. B., Charette M. P., Johnson T. V., Lebofsky L. A., and Pieters C. (1972) Spectrophotometry (0.3 to 1.1 micron) of proposed Apollo lunar landing sites. The Moon 5, 52-89.

McGill G. E. (1971) Attitudes of fractures bounding straight and arcuate rilles. Icarus 14, 53-58.

McGill G. E. (1978) Graben geometry and crustral structure (abs.). NASA Tech Mem. 79729, 100-102.

Melosh H. J. (1978) The tectonics of mascon loading. Lunar Planet. Sci. Conf. 9th, p. 3513-3525.

Metzger A. E., Haines E. L. (1979) Thorium concentrations in the Apenninus region of the moon. In Lunar and Planetary Sci. X, p. 833-835. The Lunar and Planetary Institute, Houston.

Morrison J. J. (1970) A link between cartographic theory and mapping practice: The nearest neighbor statistic. Geographical Review, 60, 494-510.

Muller P.M. and Sjogren W. L. (1968) Mascons: Lunar mass concentrations. Science 161, 680-684.

Phillips R. J., Conel J. E., Abbott E. A., Sjogren W. L., and Morton J. B., (1972) Mascons: Progress toward a unique solution for mass distribution. J. Geophys. Res. 77, 7106-7117.

Pieters Carle (1977) Characterization of lunar basalt types--II: Spectral classification of fresh mare craters: Lunar Sci. Conf 8th, p. 1037-1048.

Pike R. J. (1974) Depth/diameter relations of fresh lunar craters: revision from spacecraft data. Geophys. Res. Lett. 1, 291-294.

Pike R. J. (1977) Size-dependence in the shape of fresh impact craters on the moon. In Impact and Explosion Cratering (D. J. Roddy, R. O. Pepin, and R. B. Merrill, eds.), Pergamon Press, New York. p. 489-510.

Quaide W. L. (1965) Rilles ridges and domes--clues to maria history. Icarus 4, 374-389.

Schaber G. G. (1973) Lava flows in Mare Imbrium: Geologic evaluation from Apollo orbital photography. Proc. Lunar Sci. Conf. 4th, p.73-72.

Schultz, P. H. (1976a) Floor-fractured lunar craters. Moon, 15, 241-273.

Schultz, P. H. (1976b) Moon morphology. University of Texas Press, Austin. 626pp.

Scott D. H., Diaz J. M., and Watkin J. A. (1975) The geologic evaluation and regional synthesis of metric and panoramic photographs. Proc. Lunar Sci. Conf. 6th, p. 2531-2540.

Scott D. H., McCauley J. F., and West M. N. (1977) Geologic map of the west side of the moon. U.S. Geol. Survey Misc. Geol. Inv. Map I-1034.

Smith G. K. (1966) A comparison of two terrestrial graben with the lunar rilles Rima Ariadaeus and rimae Hypatia I and II. U.S. Geol. Survey Astrogeol. Studies, pt.A, p.65-86.

Stripe J. G. (1968) Iron meteorites as mascons. Science 162, 1402-1403.

Strom R. G. (1972) Lunar mare ridges, rings and volcanic ring complexes. Modern Geology 2, 133-157.

Swanson D. A. and Peterson D. W. (1972) Partial draining and crustal subsidence of Alae lava lake. U.S. Geol. Survey Prof. Paper 800 C, p. 1-14.

Thurber C. H. and Solomon S. C. (1978) An assessment of crustal thickness variations on the lunar near side: models, uncertainties, and implications for crustal differentiation. Lunar Planet. Sci. Conf. 9th, p 3481-3498.

Tjia H. D. (1970) Lunar wrinkle ridges indicative of strike-slip faulting. Bull. Geol. Soc. Am. 81, 3095-3100.

Urey H. C. (1968) Mascons and the history of the moon. Science 162, 1408-1410.

Whitaker E. A. (1966) The surface of the moon. In The Nature of the Lunar Surface (W. N. Hess, D. H. Menzel, and J. A. O'Keefe, eds.), p.79-98. John Hopkins, Baltimore.

Whitford-stark J. L. and Head J. W. (1977) The Procellarum volcanic complexes: Contrasting styles of volcanism. Lunar Sci. Conf. 8th, p. 2705-2724.

Wilhelms D. E. and McCauley J. F. (1971) Geologic map of the near side of the moon. U.S. Geol. Surv. Misc. Inv. Map I-703.

Wise D. U. and Gates M. T. (1970) Mascons as structural relief on a lunar "Moho." J. Geophys. Res. 75, 261-268.

Figure Captions

Fig. 1. External rim height as a function of crater diameter determined from fresh appearing lunar craters (Pike, 1977).

Fig. 2. Method for determining basalt thickness in the vicinity of a flooded crater. Estimate ignores local variation in the center of the crater and the rim.

Fig. 3. Location of interior data points used to construct the isopach map. Numbers in parentheses are arbitrary estimates in thick lenses which allow competion of the contouring program.

Fig. 4. Isopach map of the western mare basalt. Isopach interval is 250m. Regions of insufficient data are shown with diagonal ruled pattern.

Fig. 5. Provinces of the lunar western maria as defined in this paper.

Fig. 6. Model topography of the western portion of the moon. 12th degree harmonic topographic model after Bills and Ferrari (1977) Contour interval is 500 m.

Fig. 7. Model paleotopography derived by subtracting the isopach map from model topography. Contour interval is 500 m.

Fig. 8. Sketch map of major mare surface features. Compare surface trends with figs. 6 and 7 for possible spatial correlations.

Fig. 9. Location of probable impact basins in the western maria. Dots mark approximate location of outer ring and inner ring if identified. Arcs of depressed terrain outside the circular basins are indicated by dotted line with arrows.

Fig.10. Basalt thickness map derived on the assumption that all superisostatic loading in mare basins can be attributed to mare basalt. (Thurber and Solomon, 1978). Isopach interval is 500 m.

TABLE I. Point Distribution Coefficient by Mare Province

Province	Number of Points	Area (deg.^{2})/ No. of Points	Distribution Coefficient
N. Procellarum	37	29.4	1.03
E. Procellarum	8	50.0	0.90
W. Procellarum	61	32.7	0.87
Imbrium	54	29.8	1.06
Central Lowland	42	14.9	1.09
Humorum	27	11.1	0.91
Nubium	48	11.5	1.03
(Palus Epidemiarum)	16	4.7	1.39
"Whole Map"	294	13.7	1.20

TABLE II. Probable Circular Basins

Basin	Location		Diameter (km)	
	Lat. (°)	Long. (°)	Outer Ring	Inner Ring
Imbrium	36N	16W	1350	620
Stadius-Aestuum	12N	13W	720	490
E. Procellarum	23N	36W	710	---
NW. Procellarum	8N	59W	700	200
Near Struve	27N	72W	675	315
SW. Procellarum	6S	43W	550	---
Humorum	24S	39W	460	270
W. Nubium	24S	22W	410	200
E. Nubium	23S	10W	370	180
NW. Cognitum	10S	24W	290	---
Iridium	45N	31W	260	---
Medii	0	1E	250	---
Vaporum	13N	3E	240	---
SE. Cognitum	12S	21W	200	---

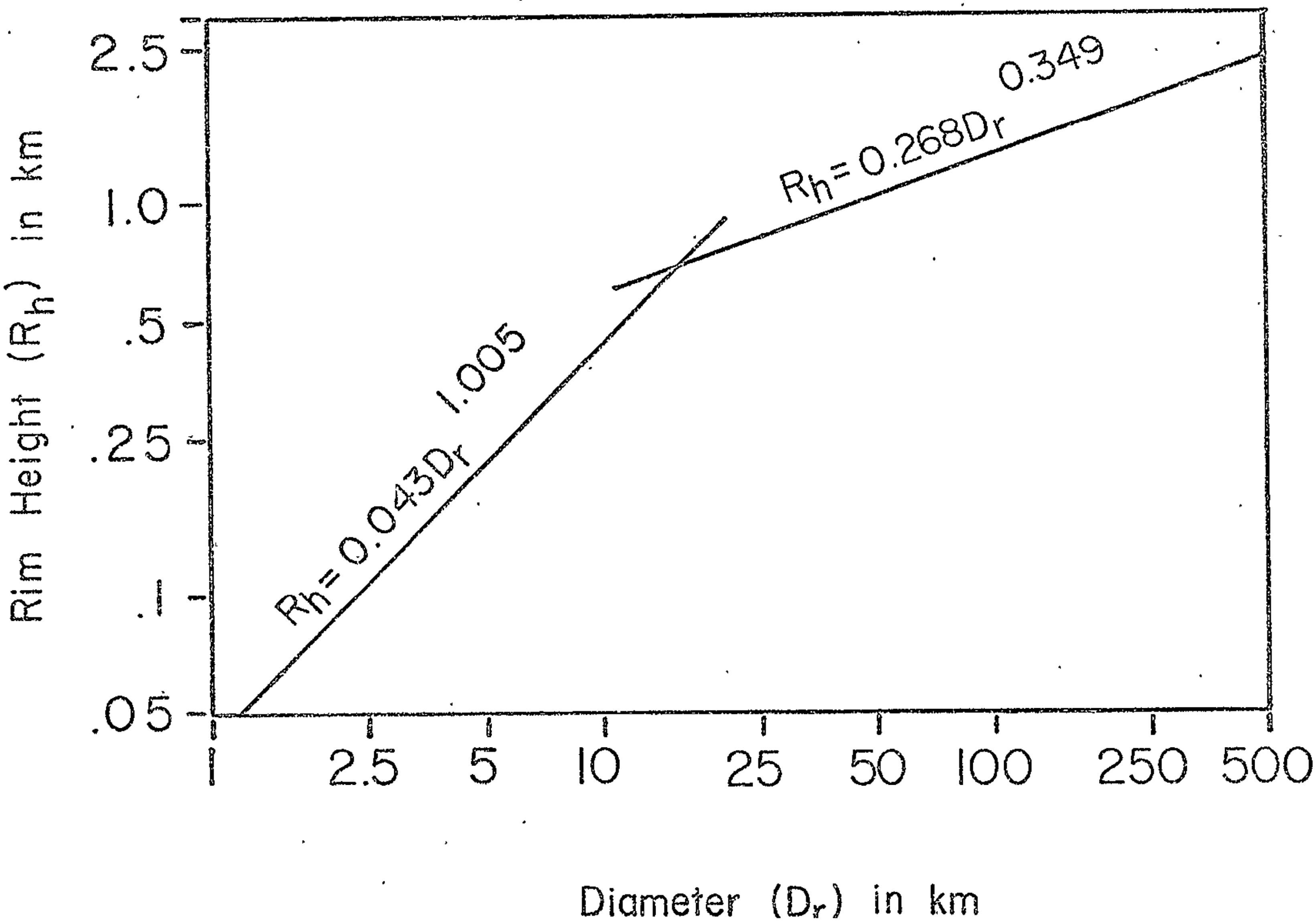

Rim Height (R_h) in km
2.5
1.0
.5
.25
.1
.05
$R_h = 0.268 D_r^{0.349}$
$R_h = 0.043 D_r^{1.005}$
1
2.5
5
10
25
50
100
250
500
Diameter (D_r) in km

FIGURE 1

$$R_h - R_e = T$$

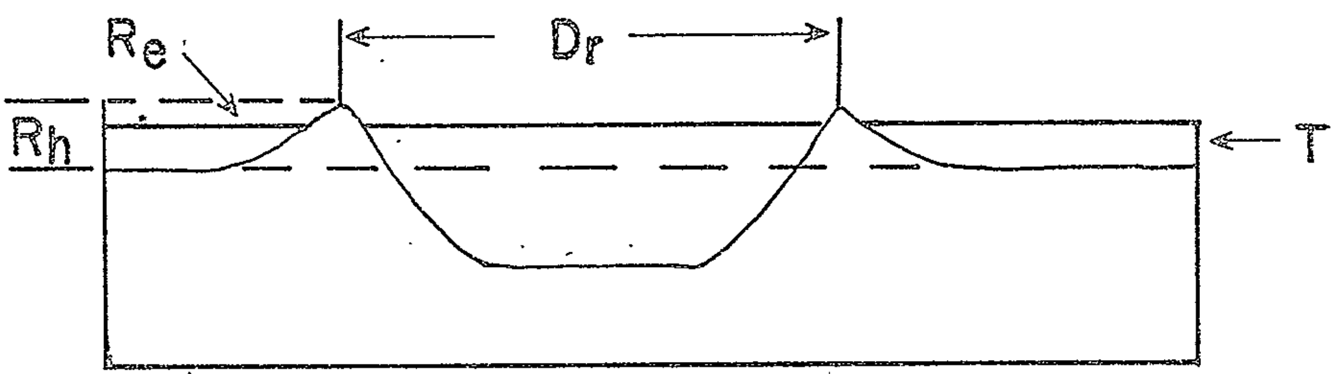

R_h = Rim Height

R_e = Exposed Rim Height

T = Thickness of Mare

Figure 2

FIGURE 3

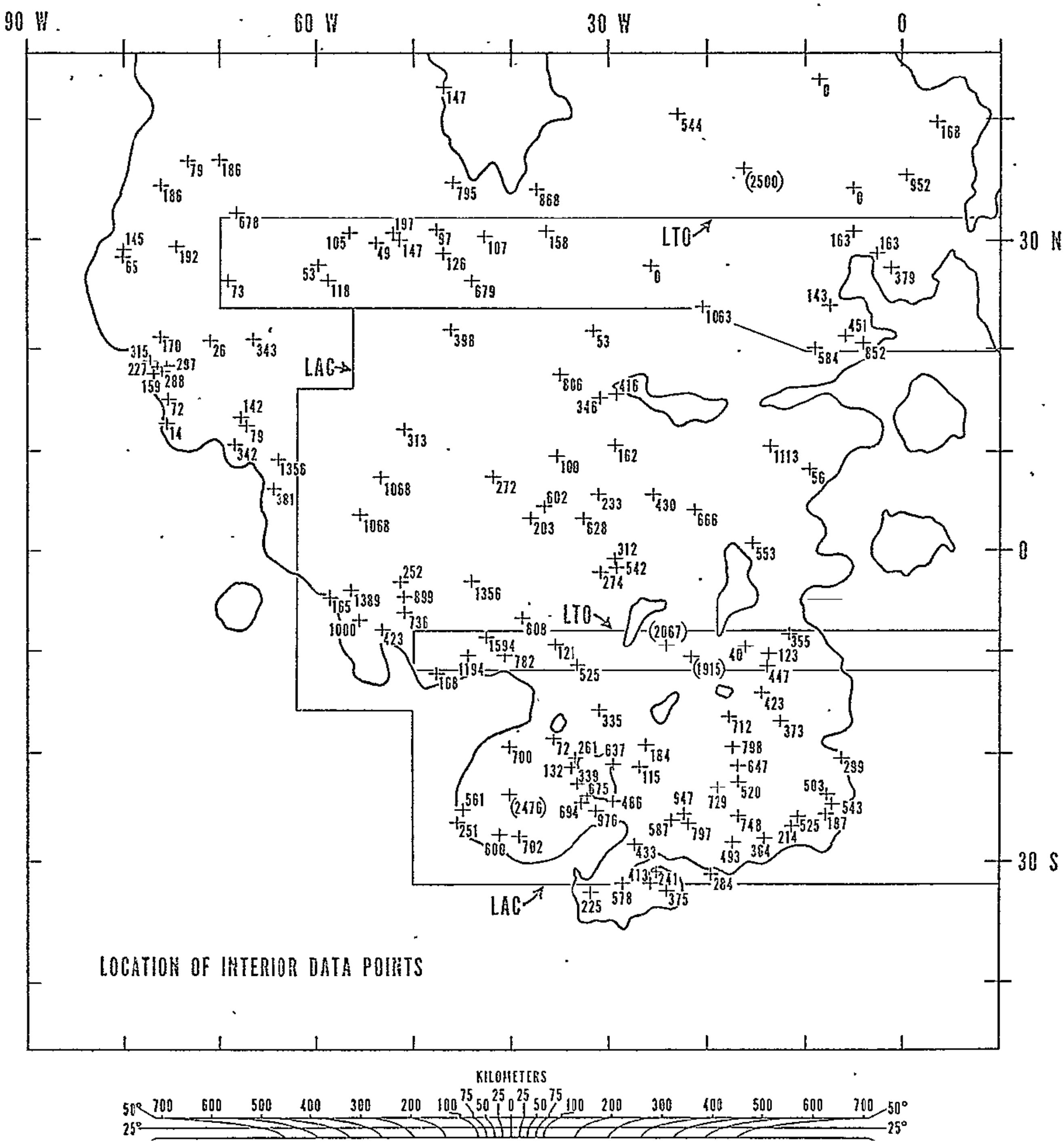
90 W
60 W
30 W
0
30 N
0
30 S
LTO
LAC
LTO
LAC
LOCATION OF INTERIOR DATA POINTS
KILOMETERS

Figure 4

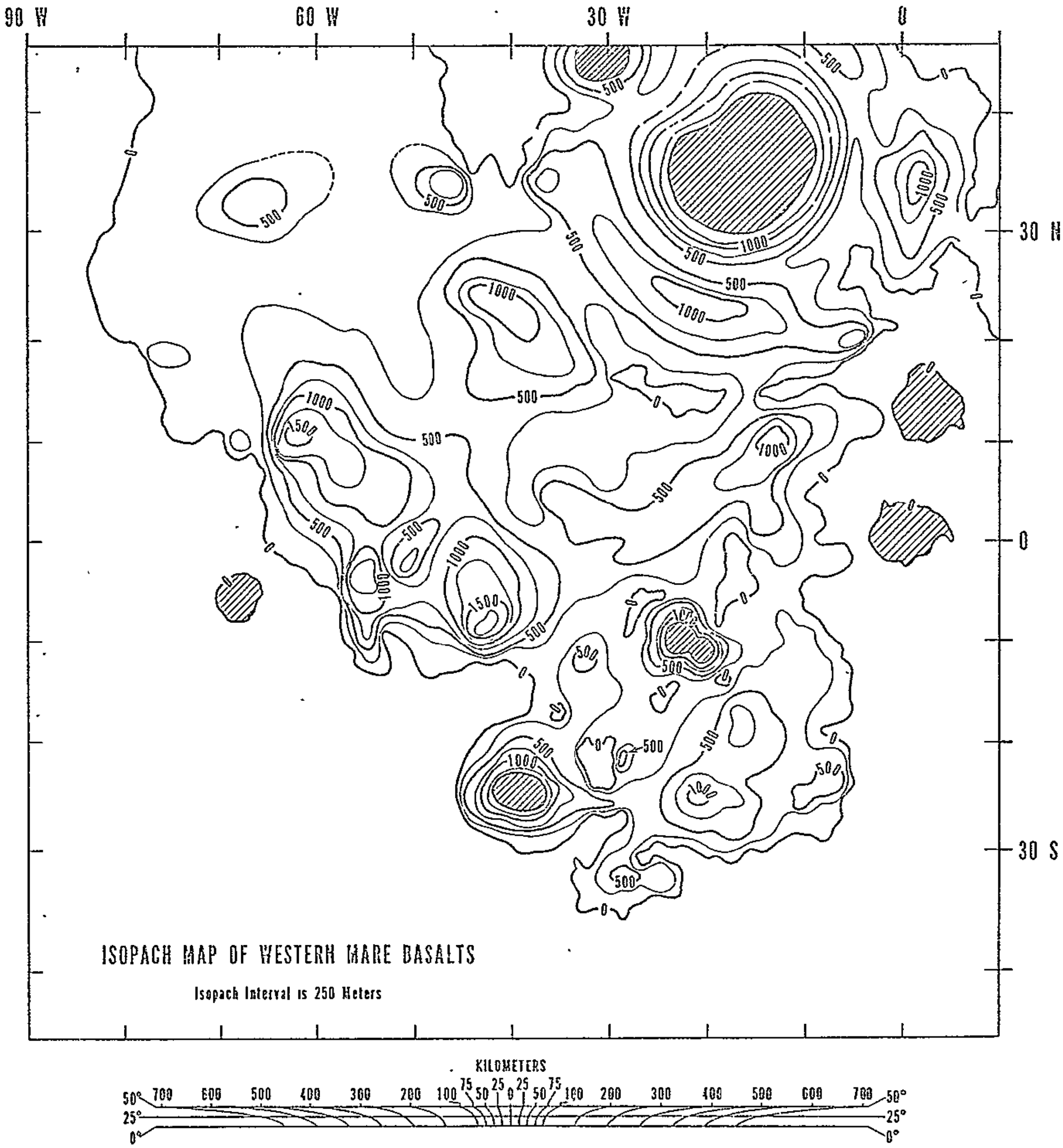
90 W
60 W
30 W
0
30 N
0
30 S
ISOPACH MAP OF WESTERN MARE BASALTS
Isopach Interval is 250 Meters
KILOMETERS
700 600 500 400 300 200 100 75 50 25 0 25 50 75 100 200 300 400 500 600 700
50°
25°
0°

FIGURE 5

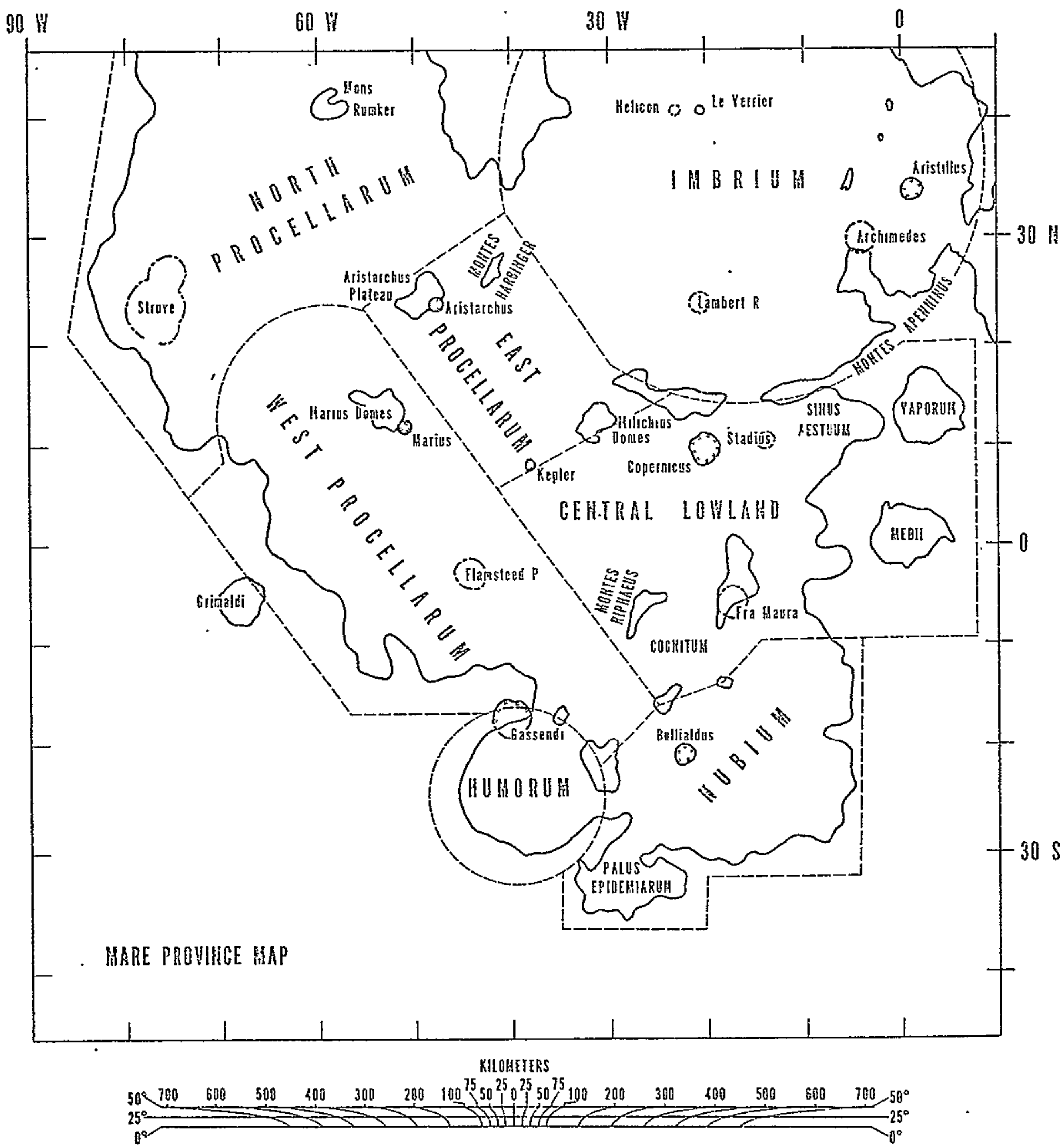

90 W
60 W
30 W
0
30 N
0
30 S
Mons Rumker
NORTH PROCELLARUM
Helicon
Le Verrier
IMBRIUM
Aristillus
Archimedes
MONTES HARBINGER
Aristarchus Plateau
Aristarchus
Struve
Lambert R
EAST PROCELLARUM
MONTES APENNINUS
WEST PROCELLARUM
Marius Domes
Marius
Milichius Domes
Stadius
SINUS AESTUUM
VAPORUM
Copernicus
Kepler
CENTRAL LOWLAND
MEDII
Flamsteed P
MONTES RIPHAEUS
Grimaldi
Fra Maura
COGNITUM
Gassendi
Bullialdus
NUBIUM
HUMORUM
PALUS EPIDEMIARUM
MARE PROVINCE MAP
KILOMETERS
700 600 500 400 300 200 100 75 50 25 0 25 50 75 100 200 300 400 500 600 700
50° 25° 0°

FIGURE 6

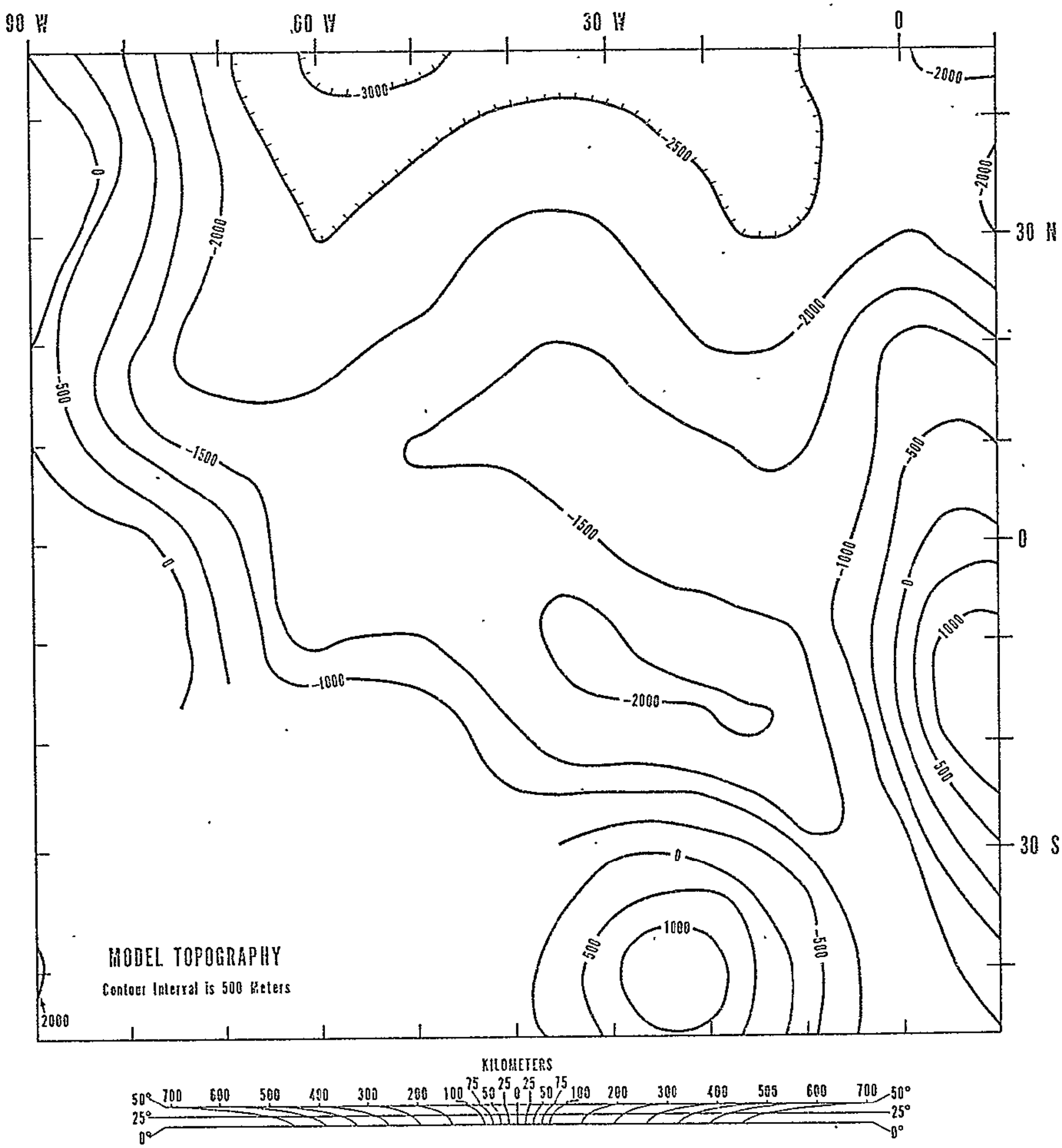
90 W
60 W
30 W
0
30 N
0
30 S
-3000
-2000
-2500
-2000
-2000
-2000
0
-500
-1500
-1500
-1000
-500
0
1000
500
-1000
-2000
0
500
1000
-500
2000
MODEL TOPOGRAPHY
Contour Interval is 500 Meters
KILOMETERS
50° 700 600 500 400 300 200 100 75 50 25 0 25 50 75 100 200 300 400 500 600 700 50°
25° 25°
0° 0°

FIGURE 7

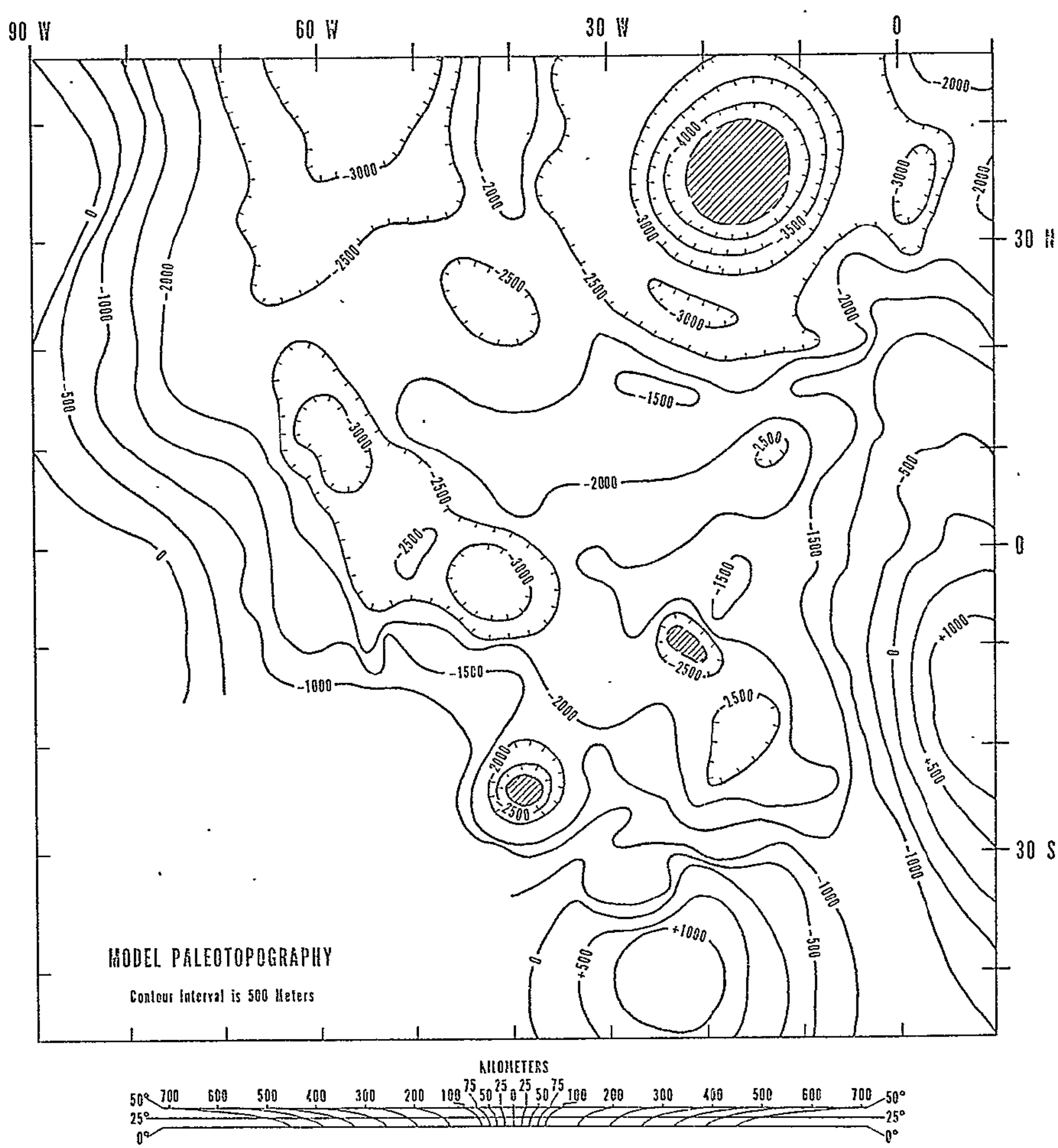
90 W
60 W
30 W
0
30 N
0
30 S
-2000
-3000
-2500
-1000
-500
0
-4000
-3500
-1500
+1000
+500
MODEL PALEOTOPOGRAPHY
Contour Interval is 500 Meters
KILOMETERS
50°
25°
0°
700
600
500
400
300
200
100
75
50
25

FIGURE 8

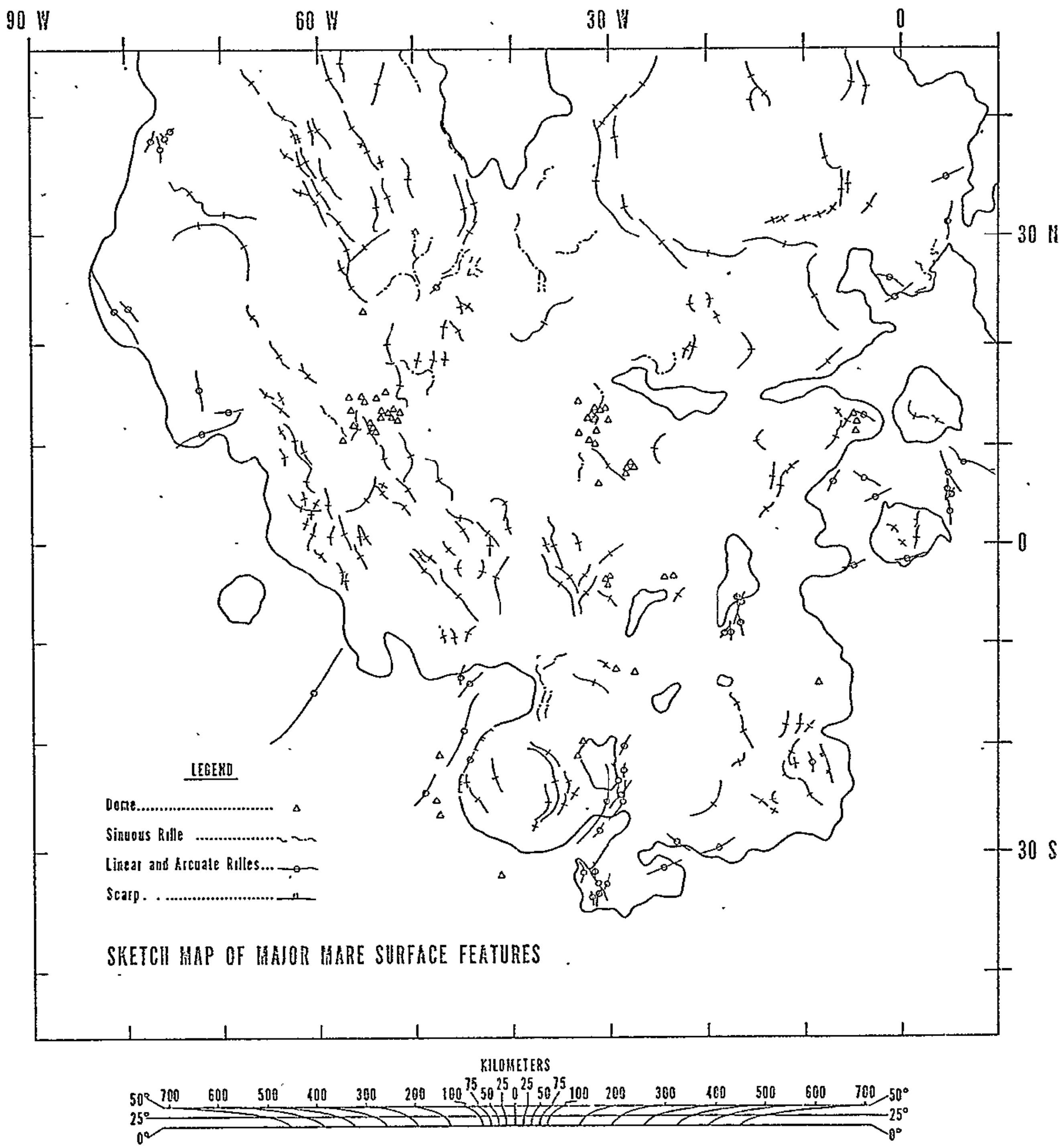

SKETCH MAP OF MAJOR MARE SURFACE FEATURES

FIGURE 9

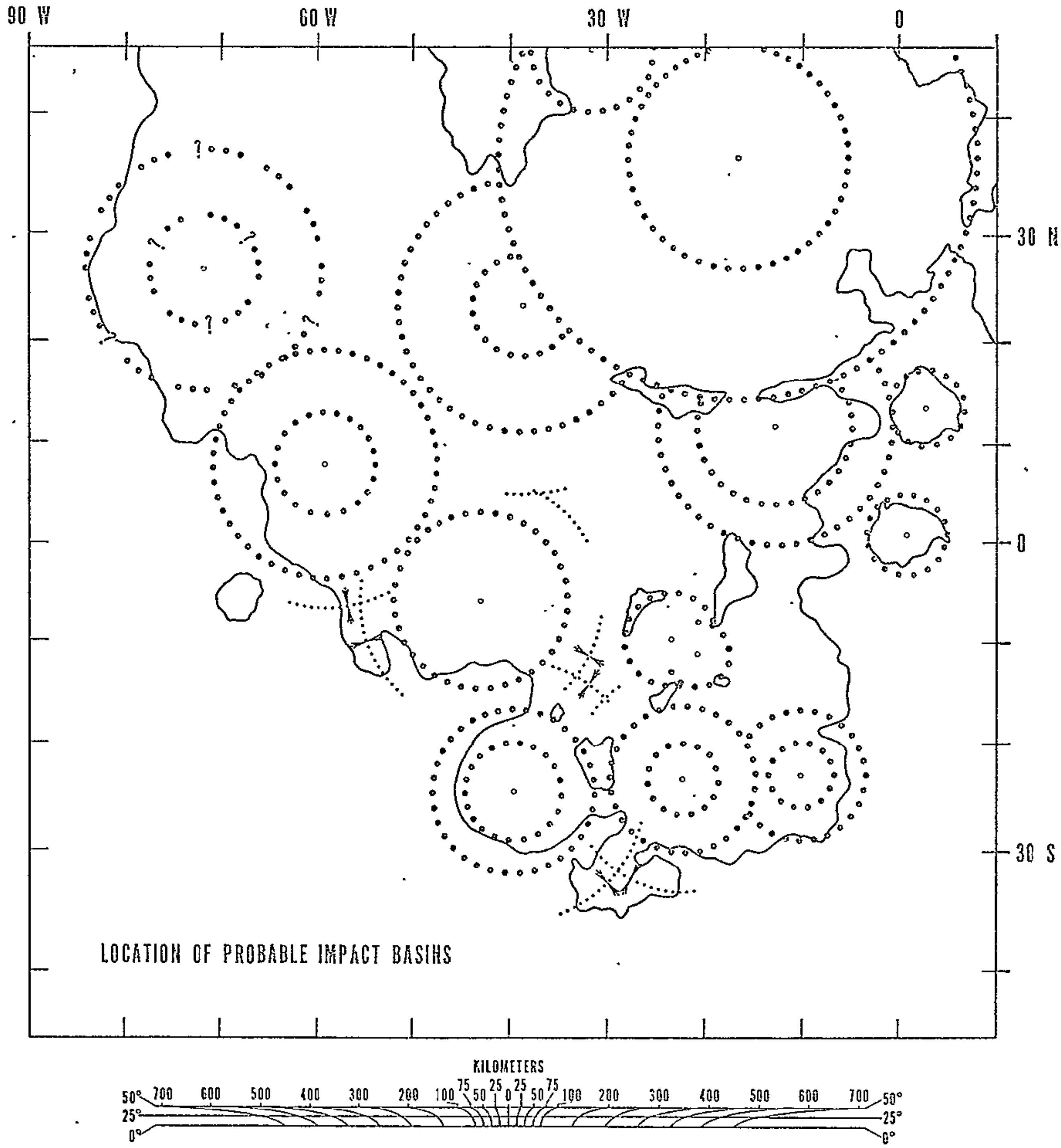
90 W
60 W
30 W
0
30 N
0
30 S
LOCATION OF PROBABLE IMPACT BASINS
KILOMETERS
50°
25°
0°
700
600
500
400
300
200
100
75
50
25
0
25
50
75
100
200
300
400
500
600
700
50°
25°
0°

FIGURE 10

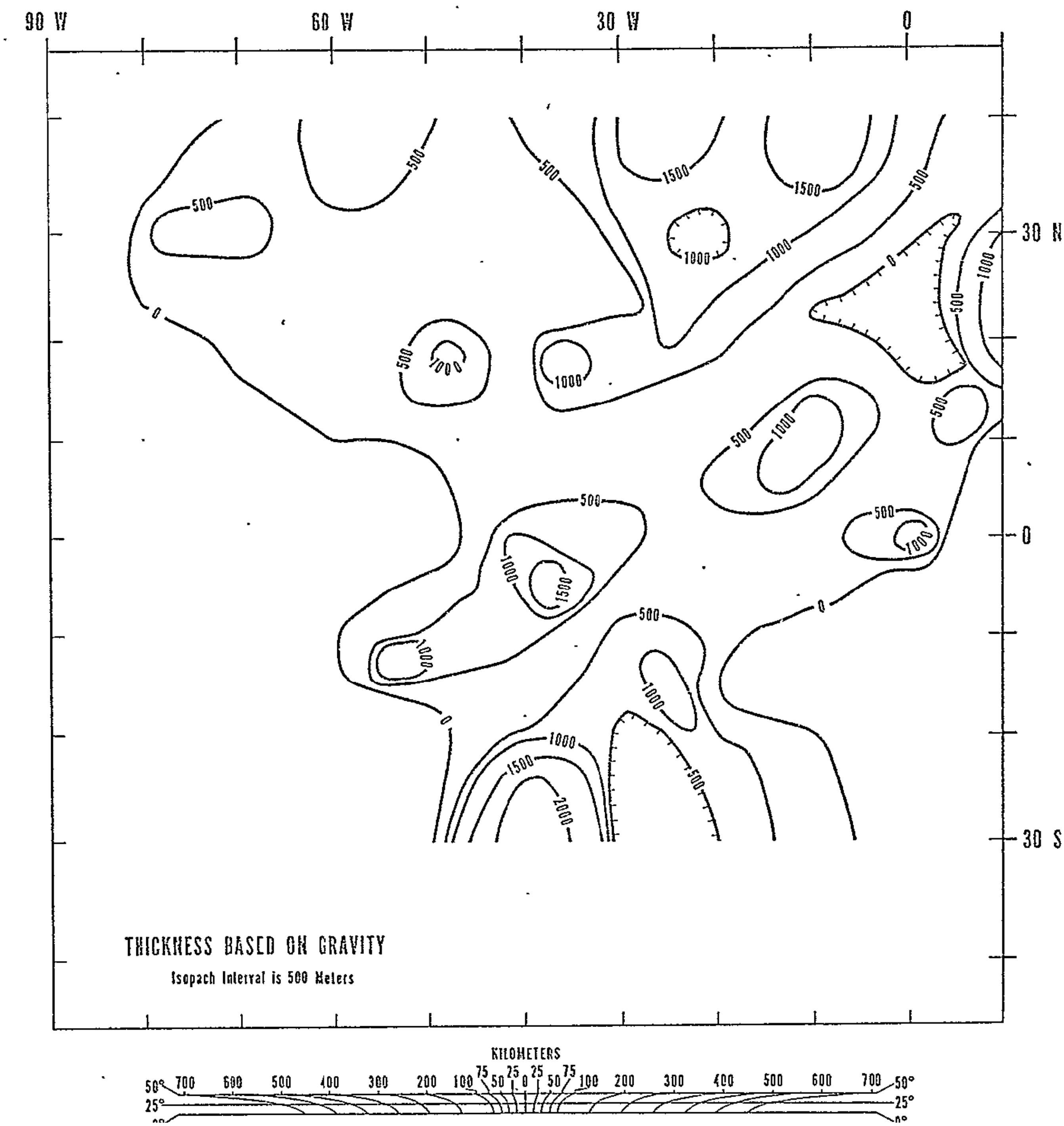

90 W
60 W
30 W
0
30 N
0
30 S
500
1500
1000
2000
0
THICKNESS BASED ON GRAVITY
Isopach Interval is 500 Meters
KILOMETERS
700 600 500 400 300 200 100 75 50 25 0 25 50 75 100 200 300 400 500 600 700
50°
25°